Batteries & Supercaps

Research Article
doi.org/10.1002/batt.202500070

Chemistry Europe
European Chemical Societies Publishing

www.batteries-supercaps.org

Long-Term Stability Evaluation of Optical Fiber Sensors Immersed in $LiPF_6$ Electrolyte

Lucca C. Matuck, Luís F. B. Fontes, Nuno F. Santos, João L. Pinto, Marta S. Ferreira, Olivier Raccurt, and Micael S. Nascimento*

Stability tests on silica optical fiber sensors (fiber Bragg gratings) within the lithium–ion battery (LiB) electrolyte are conducted, revealing their robustness over 24 months, only subject to variations in ambient temperature. Recurrent chemical analyses based on scanning electron microscopy and energy-dispersive X-ray spectroscopy characterizations demonstrate the formation of deposits ($LiPF_6$ crystals) from electrolyte decomposition in the fiber surfaces over time. However, no silica material degradation is observed. The performance and accuracy of the optical fiber sensors are tested before and after aging, revealing an insignificant variation in their thermal sensitivity, with values within the measurement error. This research demonstrates the durability and the potential of this advanced sensing technology in the field of LiB monitoring, making a substantial contribution to the domain of sustainable energy solutions. It offers invaluable insights for enhancing LiB safety, reliability, and overall performance, ultimately advancing the integration of LiBs within our evolving sustainable energy landscape.

1. Introduction

The increasing demand for efficient and sustainable energy storage solutions has driven substantial advancements in battery technology. Among the various types of batteries, lithium–ion batteries (LiB) have gained significant attention due to their high energy density, long cycle life, and low self-discharge rate.[1] These attributes make LiBs a preferred choice for numerous applications, including electric vehicles, grid storage, and portable electronics.[2,3]

As the deployment of LiBs expands, the need for effective monitoring and maintenance systems becomes paramount.[4,5] Between all the new advanced sensing technologies applied to energy storage systems, optical fiber sensors (OFS), particularly those inscribed in silica optical fibers, have been proposed as valuable tools.[6,7] Among these sensors, fiber Bragg gratings (FBGs), inscribed in the core of the photosensitive silica optical fibers, are particularly noteworthy for their ability to monitor in real time various internal parameters of batteries, such as temperature, strain, and/or pressure.[8–13] The capability of FBGs to monitor these parameters shows promise in enhancing the safety, efficiency, and longevity of battery systems.[14–16] While laboratory experiments suggest potential benefits, the integration of OFS in commercial battery systems is still at an early stage, requiring further validation and industrial adoption.[17–22]

OFS offers several advantages for battery monitoring. They are immune to electromagnetic interference, have a small size, and can be embedded within battery packs to provide distributed sensing capabilities.[23,24] However, despite these advantages, there is a need to understand the long-term stability and performance of these sensors and the corresponding silica material of the optical fiber when exposed to the internal chemical environment of the batteries. The LiB electrolytes, for instance, due to their harsh compounds, can potentially affect the integrity and functionality of the silica optical fibers. Over time, chemical interactions between the electrolyte and the optical fiber may lead to degradation, potentially impacting the accuracy and reliability of the sensor readings.

Previous studies have investigated the stability of FBGs embedded in LiBs.[25,26] However, these studies primarily focused on changes in the FBGs thermal sensitivity over time, without conducting any chemical analysis. Notably, they observed no significant changes in thermal sensitivity during an analysis period of just six months of exposure.

INSTABAT,[27] a project within the Battery 2030+ roadmap,[14] explores using and developing OFS in battery applications to monitor internal safety parameters. Given the limited understanding of electrolyte effects on OFS, this work aims to provide reliable insights into their feasibility and performance within battery environments. The objective of this work is to address the impact of the electrolyte on the stability of OFS. These findings will contribute to advancing the integration of these sensors into battery cells, aligning with the goals outlined in the BATTERY2030+ roadmap.

L. C. Matuck, N. F. Santos, J. L. Pinto, M. S. Ferreira, M. S. Nascimento
i3N and Department of Physics
University of Aveiro
Campus de Santiago, 3810-193 Aveiro, Portugal
E-mail: micaelnascimento@ua.pt

L. F. B. Fontes
CICECO-Aveiro Institute of Materials,LAQV-REQUIMTE,Department of Chemistry
University of Aveiro
Campus de Santiago, 3810-193 Aveiro, Portugal

O. Raccurt
DEHT
University Grenoble Alpes, CEA, LITEN
F-38000 Grenoble, France

Supporting information for this article is available on the WWW under https://doi.org/10.1002/batt.202500070

This work investigates the degradation of single-mode fibers (SMF), commonly used in long-term LiB monitoring,[15,28,29] and evaluates the behavior of FBG sensors inscribed in polarization-maintaining single-mode silica fibers (PM-SMF). Long-term stability tests were conducted, with periodical analyses through scanning electron microscopy (SEM) and energy-dispersive X-ray spectroscopy (EDS). This study represents an initial effort to assess the impact of exposing silica fibers to LiB electrolytes under controlled conditions, providing critical insights into their behavior. While the effect of temperature variations within real battery cells is not addressed here, these results offer a foundation for future studies aiming to evaluate the stability of OFS in more representative environments. Understanding the degradation mechanisms and their implications on sensor functionality is essential for the development of robust and dependable monitoring systems for next-generation batteries.

2. Experimental Section

2.1. OFS Production and Characterization

An FBG sensor consisted of a periodic modulation of the refractive index in the core of an optical fiber. When light coming from a broadband optical source was guided through an FBG, a narrow band of wavelengths was selectively reflected, while all other wavelengths were transmitted with minimal loss.[30] The reflected wavelength, known as the Bragg wavelength (λ_{FBG}), was highly dependent on the grating intrinsic characteristics, such as its period, length, and the strength of refractive index modulation. This relationship is described by the Bragg condition in Equation (1).

$$\lambda_{FBG} = 2n_{eff}(T)\Lambda(T) \tag{1}$$

where n_{eff} is the effective refractive index of the fiber core, Λ is the grating period, and T is the temperature. The reflected wavelength shifted in response to external changes, making FBGs valuable for sensing applications. From Equation (1), the λ_{FBG} dependence on temperature can be estimated according to the following.

$$\frac{\partial \lambda_{FBG}}{\partial T} = \lambda_{FBG}\left(\frac{1}{\Lambda}\frac{\partial \Lambda}{\partial T} + \frac{1}{n_{eff}}\frac{\partial n_{eff}}{\partial T}\right) \tag{2}$$

where $\frac{1}{n_{eff}}\frac{\partial n_{eff}}{\partial T}$ corresponds to the thermo-optic effect coefficient and $\frac{1}{\Lambda}\frac{\partial \Lambda}{\partial T}$ is the thermal expansion coefficient. These two parameters had a typical value of 8.5×10^{-6} and $0.55 \times 10^{-6}\,°C^{-1}$, respectively, for silica fibers.[31]

The manipulation of the optical fiber geometry could enhance certain properties of light. For instance, PM-SMFs were specifically designed to preserve the polarization state of light as it traveled through the fiber, minimizing cross-talk between polarization modes. These fibers exhibited two principal axes, with different refractive index distributions, which affected the speed of light. These axes were commonly referred to as the fast axis (higher effective refractive index, $n_{eff,f}$) and the slow axis (lower effective refractive index, $n_{eff,s}$). The difference between the effective refractive index was called birefringence. In PM-SMFs, it can be evaluated using the following equation.

$$B(T) = n_{eff,f}(T) - n_{eff,s}(T) \tag{3}$$

When a FBG was inscribed in a PM-SMF, due to the high-birefringence, two Bragg wavelengths appeared in the reflection spectra, each governed by the Bragg condition presented in Equation (1). On the other hand, since the thermal expansion coefficient is much lower than the thermo-optic coefficient, and taking Equation (1) into consideration, we obtain the following.

$$B(T) = \frac{\lambda_{FBG,f}(T) - \lambda_{FBG,s}(T)}{2\Lambda} \tag{4}$$

Thus, by monitoring the changes in the Bragg wavelength, it was possible to estimate the evolution of the fiber birefringence over time, which could be an indicator of structural changes in the optical fiber.

Figure 1 presents the cross-section images of a standard SMF with a ≈9.8 μm core and the PANDA fiber used in this work. For comparison purposes, it also showed the reflection spectra of two FBGs: one inscribed in the SMF, where a single peak is observed, and the other one inscribed in the PM-SMF (PANDA) fiber, where the two aforementioned peaks arose. The difference in wavelength between these peaks depended on the birefringence magnitude, which was determined by the fiber's geometry and the core material properties (Figure 1). Using this type of fiber also allowed the researchers to easily assess the effects of electrochemical etching, as birefringence created asymmetries between the fast and slow axes. The inherent birefringence of PM-SMF made it easier to early detect possible external perturbations performed in the fiber core material, and this could be highlighted if an FBG sensor was recorded near the fiber tip, providing enhanced accuracy in monitoring structural modifications, if occur.

In this study, two FBG sensors (≈10.0 mm length) were sequentially inscribed in a section of PANDA fiber, previously submitted to a hydrogenation process over 2 weeks.[12] The FBG inscription process utilized a pulsed Q-switched Nd:YAG laser system (LOTIS TII LS-2137U Laser, Minsk, Belarus), operating at its fourth harmonic (266 nm). The laser beam was focused onto the fiber using a plano-convex cylindrical lens with a working length of 320 mm. To produce FBGs with distinct wavelength peaks (1537 and 1551 nm), phase masks with different grating periods, supplied by Ibsen, were employed.

The different wavelengths enable easy tracking of the changes that occur on each FBG independently.[10]

Both FBGs were calibrated after and before the experiment for temperature in a climatic chamber (WeissTechnik LC64, with an operating range from −70.0 to 180.0 °C) by applying a 5.0 °C increment between 20.0 ± 0.1 and 30.0 ± 0.1 °C to not affect the electrolyte solution. Additionally, the temperature of the climatic chamber was monitored using a calibrated thermocouple (TC) to ensure precise readings, with its measurements plotted alongside the FBG response to validate the consistency of the chamber's conditions.

Research Article
doi.org/10.1002/batt.202500070
Chemistry Europe
European Chemical Societies Publishing

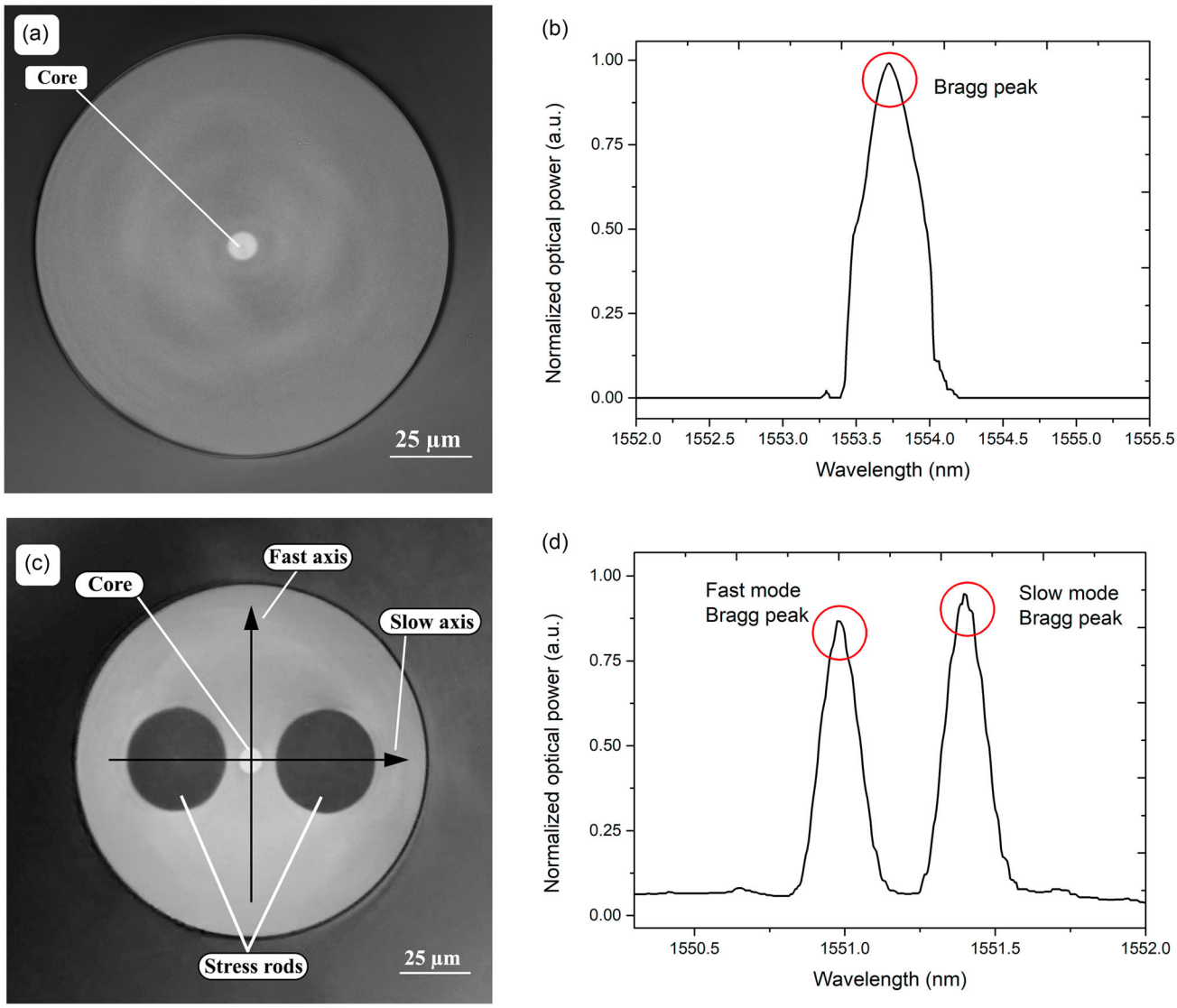

Figure 1. a) Cross-section image of a silica SMF. b) Spectral response of a FBG inscribed in a bare SMF, showing a single Bragg peak. c) Cross-section image of the silica PM-SMF in PANDA configuration used in the experiment, where birefringence is induced by stress rods aligned along the fast and slow axes. d) Spectral response of a FBG inscribed in a PM-SMF, showing two distinct Bragg wavelengths corresponding to the fast and slow modes.

To correlate the Bragg wavelength with temperature shifts, the following equation can be used.

$$\lambda_{FBG}(T) = kT + \lambda_0 \tag{5}$$

where k is the sensitivity in pm °C^{-1} and λ_0 is the Bragg wavelength when $T = 0$ °C.

$$B(T) = n_{ef,f}(T) - n_{ef,s}(T)B = \frac{\lambda_{FBG,f}(T) - \lambda_{FBG,s}(T)}{2\Lambda} \tag{6}$$

2.2. Silica Optical Fiber Probes Preparation for Stability Tests in LiB Electrolyte

The degradation assessment of both silica SMF (without a sensing element) and PM-SMF with the FBG sensors was carried out by exposing the samples to the harsh chemical environment within the LiB electrolyte. On the one hand, this evaluation involved introducing small amounts of the electrolyte solution used in the framework of the INSTABAT project (EC/EMC), in a 3:7 vol. ratio, consisting of 1 M $LiPF_6$ + 2% VC, sourced from MU Ionic Solutions Co (Japan) and provided by CEA) into 12 specially designed aluminum-compatible flasks, together with one SMF section per flask (of about 3 cm in length), which became submerged in the electrolyte. This process was performed inside a nitrogen-pressurized glove box to maintain a controlled environment, ensuring all safety procedures and avoiding the contamination of the electrolyte during the insertion. On the other hand, the PM-SMF with the two FBGs was positioned in such a way that each FBG would be surrounded by a different environment. The FBG@1537 nm was submerged in the liquid electrolyte, while the FBG@1551 nm was positioned in the gas phase above the electrolyte, as illustrated in **Figure 2**.

Research Article
doi.org/10.1002/batt.202500070
Chemistry Europe
European Chemical Societies Publishing

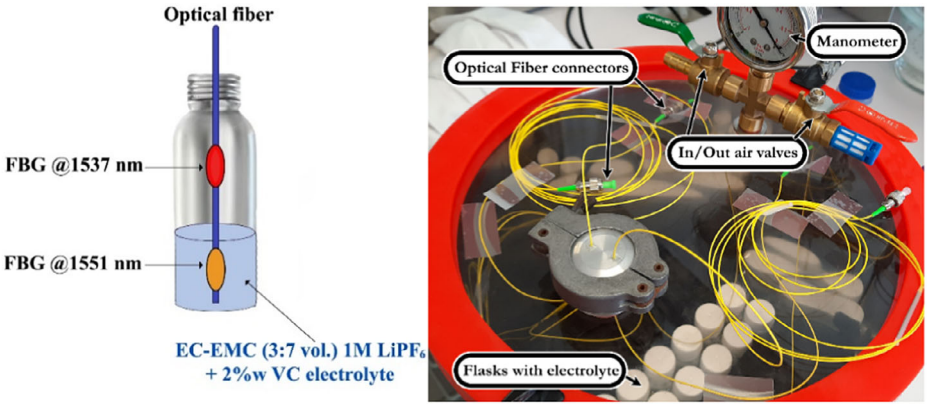

Figure 2. Left: representation of the FBGs arrangement in a flask partially filled with EC-EMC (3:7 vol.) 1M LiPF6 + 2%w VC electrolyte. Right: photograph showing the air-sealed container along with the flasks and external instrumentation used to control the internal pressure.

Throughout the 24 month-long experiment, the flasks were securely stored in a nitrogen-rich atmosphere inside an air-sealed container placed in a fumehood to minimize oxidation and maintain sample stability.

Periodically, the SMFs exposed to the liquid electrolyte were retrieved for SEM and EDS analysis to evaluate the extent of corrosion and chemical deposition. The optical fibers analyzed with SEM were not resubmerged into the electrolyte after the analysis. To ensure a controlled study over time, multiple optical fiber samples were prepared and stored in 12 separate flasks, allowing for sequential analyses at different time points over the 24 months. This approach ensured that each analyzed fiber was only exposed to the electrolyte once, preventing any potential interference from the carbon coating or handling effects on subsequent measurements. These analyses were conducted using a TESCAN Vega3 SBH SEM microscope equipped with a Bruker Xflash 410 M Silicon Drift X-ray Detector, which has an energy resolution of 133 eV@ MnK (100 k cps). Elemental mappings and quantifications were performed using Bruker's ESPRIT software, employing a standardless P/B ZAF algorithm. These analyses were performed to understand if any corrosion and/or chemical deposition on the fiber surfaces occurs over time.

The protocol for preparing the fibers for SEM analysis involved minimal handling to preserve the integrity of the samples and the deposits formed during the experiment. After removing the fibers from the electrolyte, they were exposed to air briefly during the transfer process. No cleaning procedure was performed on the fiber surfaces before the SEM analysis to avoid altering the deposition patterns. To facilitate SEM imaging analysis, a thin carbon layer was deposited on the fiber surfaces to provide an electrically conductive coating, essential for suppressing charge accumulation. This step, along with the sample transfer and preparation, was completed within a few hours (≈1–2 h) after the fibers were removed from the electrolyte. While these interactions with air were unavoidable, the consistent preparation protocol ensures that the observed deposits are primarily attributed to the exposure of the fiber to the electrolyte during the experiment, rather than artifacts introduced during the handling process.

FBG sensor spectral response measurements were conducted every 15 days for 24 months using an optical interrogator (Hyperion si155, LUNA, Atlanta, GA, USA) with a spectral range of 1460.0–1620.0 nm. These measurements aimed to detect any changes in the signals of the FBG sensors' spectral characteristics due to chemical exposure and/or birefringence differences on the double peaks of the FBG sensors.

3. Results and Discussion

3.1. Stability Tests of FBG Sensors in PM-SMF Fibers Over Time

To evaluate the stability of the FBG sensors inscribed in PM-SMF under exposure to battery electrolyte, measurements were performed over 24 months, with the sensors subjected only to natural variations in environmental temperature. The wavelength shifts from both FBG sensors were converted to temperature values (via Equation (5)), with the results shown in the (Figure S1, Supporting Information). The trend follows the environmental temperature fluctuations, and the difference between the ambient temperature measured by the TC and the temperature recorded by the FBG sensors was plotted as ΔT for both sensors to investigate this variation (see **Figure 3**a). A discrepancy value of ≈0.16 °C was registered within the measurement error.

The ambient temperature monitoring was performed using a K-type TC integrated into the station, which has a measurement error of ±1.0 °C. The TC was placed in a different location from the IFBG sensors, as the experiment was conducted inside a sealed box, and the TC was exposed to the station's temperature rather than the specific conditions within the bottles. This discrepancy, combined with the fact that the experiment, was not conducted under tightly controlled temperature conditions, explains the observed ΔT variations. Additionally, the sealed box was periodically opened during the experiment to retrieve samples every 3 months, which could have introduced minor shifts in temperature equilibrium.

Despite these factors, the temperature differences recorded remain within acceptable limits and do not significantly impact the reliability of the results; as shown in Figure 3a, all measurements fell within the error margin of the TC (±1.0 °C). However, these observations highlight the importance of conducting future

Research Article
doi.org/10.1002/batt.202500070
Chemistry Europe
European Chemical Societies Publishing

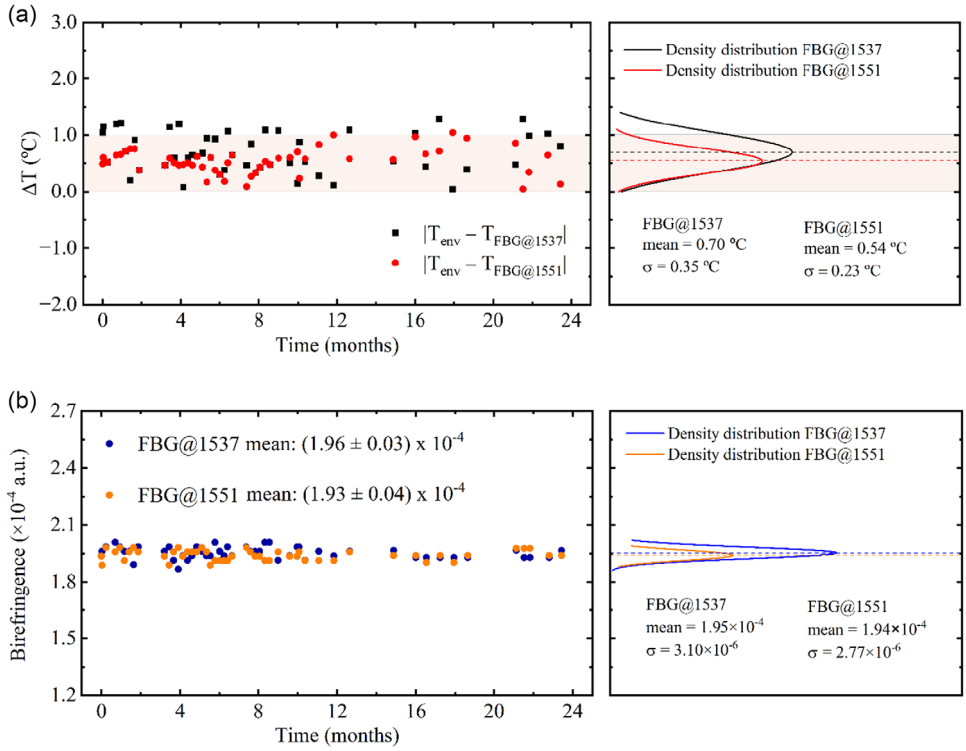

Figure 3. a) Temperature difference between the FBGs and the environmental temperature. The red shading represents the error margin of the TC sensor used in the experiment (1.0 °C resolution). b) Birefringence assessment of both FBGs throughout the experiment.

experiments under more controlled thermal conditions to minimize potential sources of variation.

Furthermore, the FBG sensor immersed in the electrolyte solution (FBG@1551 nm) demonstrated a comparable response to the non-immersed sensor (FBG@1537 nm), showing no significant deviation in performance. To further assess the impact on the FBGs, the birefringence value of the fiber was monitored throughout the test period using Equation (6), with the results presented in Figure 3b.

The periodic measurements of the optical data over the 24 months indicated that the Bragg wavelength of the FBGs remained unchanged, confirming the suitability of these sensor materials for long-term and internal battery monitoring. Additionally, **Figure 4** shows the spectral response of the FBG sensors at the beginning and end of the experiment (day 1 and day 703), revealing no significant changes in reflected wavelengths or power levels. This stability suggests that the FBGs are shielded from external chemical interactions, and no measurable effects on the fiber core were detected after 703 days of exposure. These results highlight the robustness of FBG sensors for internal battery sensing applications in harsh environments.

While the results demonstrate the robustness of the silica fibers in the liquid electrolyte under controlled conditions, it is important to note that in a real battery cell, this behavior can be significantly different. The electrolyte quantity is reduced; however, a more aggressive gaseous phase could be present due to the battery operation and higher temperatures registered over this operation. In this way, these differences could influence the integrity of the silica fiber and the performance of

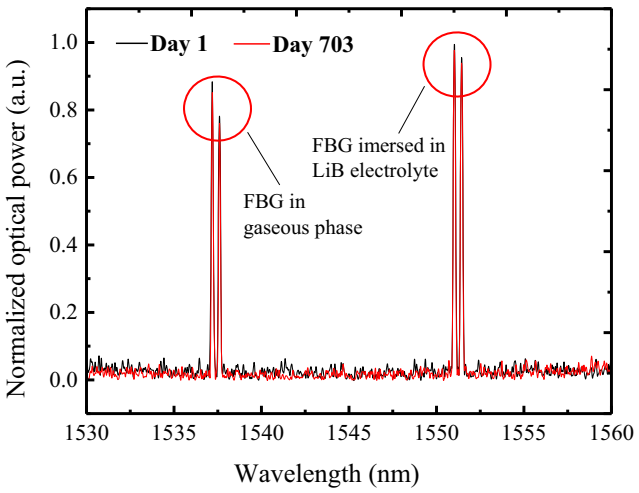

Figure 4. Spectral response of the FBG sensors inscribed in the PM-SMF on day 1 and day 703 of immersed electrolyte.

the incorporated sensors. Therefore, the findings of this study, although promising, should be viewed as an initial step. Further studies are necessary to evaluate the fiber's behavior and stability in more representative conditions, such as those found inside a battery cell during operation.

3.2. SEM and EDS Characterization of Silica SMF Over Time

Several SMFs were periodically characterized in SEM/EDS analysis to evaluate any chemical deposition on the fiber surfaces or

Research Article
doi.org/10.1002/batt.202500070
Chemistry Europe
European Chemical Societies Publishing

the possible physical degradation. A progressive formation of deposits was observed (**Figure 5**). The orange color on the mappings reflects the presence and superposition of *F* and *P* in the deposits (due to the combination of *F* in red and *P* in yellow, Figure 5f–j). Note that the fact that some deposits or crystal facets do not show any superimposed color is due to the shadowing effect, that is, obstructed or limited line-of-sight regarding the X-ray detector. In the 3rd month, cubic-like deposits are formed showing sharp edges and facets, which tend to grow in size as immersion duration is increased (Figure 5k–o). Semiquantitative point EDS measurements on these crystals (**Figure 6**) reveal the presence of *F* and *P* in a stoichiometry consistent with that of $LiPF_6$ (measured average *F*/*P* ratio of 9.0 ± 5.0), which is known to crystallize in a trigonal structure giving rise to rhombohedra that appear as cubic-like shapes as seen in Figure 5n. On the other hand, a second morphology with smaller, amorphized grains also develops (see Figure 5l–o). For these deposits, the measured *F*/*P* atomic ratio varies greatly, but it is in general increased, reaching up to 30 and above, which is reflected in the redder contrast in the EDS data. Regardless of the extensive coverage of the fiber surface by these deposits, the diameter of the fiber remains unchanged, and no signs of silica degradation were observed, and hence the integrity of the optical fiber and its core was maintained throughout the whole analyzed period.

Table 1 summarizes the elemental composition obtained from the EDS analysis of the fiber exposed to the $LiPF_6$ electrolyte. The presence of Si is attributed to the silica fiber material itself, while Al corresponds to the signal arising from the support on which the fiber was mounted for analysis. The C (carbon) signal arises from the coating applied to the fiber, providing an electrically conductive fiber surface to suppress charge accumulation effects. These observations confirm the chemical interaction between the electrolyte and the fiber's surface, but it is important to note that, despite the presence of these deposits, no visible degradation of the silica fiber was observed, reinforcing the robustness of OFS in this type of harsh environment.

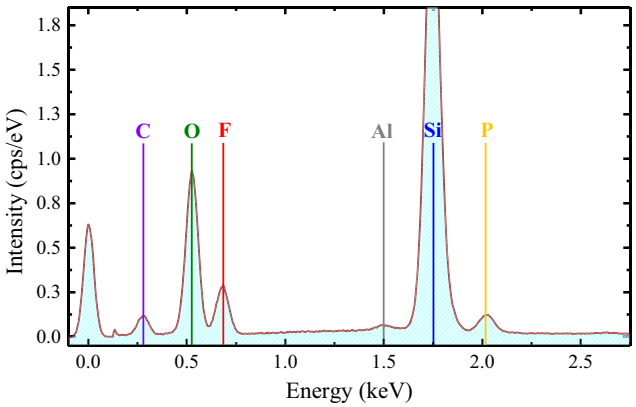

Figure 6. EDS characterization of the silica optical fiber exposed to the electrolyte after 18 months identifying the respective chemical compounds at the $LiPF_6$ crystal.

While this study demonstrates the long-term stability of OFS in LiPF6 electrolyte, real battery environments introduce additional challenges that could impact sensor performance. Temperature fluctuations, internal pressure variations, and electrode degradation may alter sensor reliability over time. In particular, thermal runaway can trigger chemical reactions within the electrolyte, generating hydrofluoric acid in the gas phase, which is highly reactive and capable of etching silica-based optical fibers. Additionally, internal pressure buildup during cell swelling may physically compromise certain OFS. Understanding these stress factors is essential for assessing the long-term durability of OFS, highlighting the need for further studies in fully assembled battery cells under operational conditions.

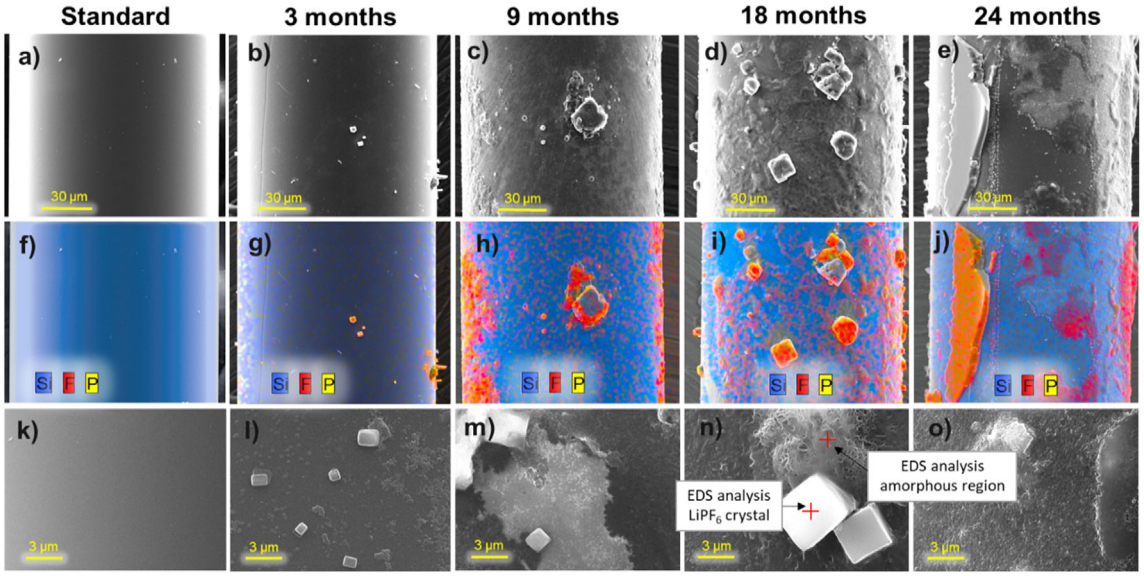

Figure 5. SEM analysis of the PM-SMF's chemical exposure over time. a–e) The secondary electron (SE) images of the fiber at 0, 3, 9, 18, and 24 exposure months, respectively. f–j) The EDS mapping images of the fiber over time. k–o) Magnified SE images of the deposits on the fiber surface.

Research Article
doi.org/10.1002/batt.202500070
Chemistry Europe
European Chemical Societies Publishing

Table 1. Elemental composition derived from EDS analysis of the fiber exposed to $LiPF_6$ electrolyte after 18 months immersed.

	Fluorine	Silicon	Phosphorus	Carbon	Oxygen	Aluminum
Atomic proportions [%]	9.85	29.35	1.09	30.73	28.44	0.55
Error [%]	5.17	7.16	0.30	17.39	13.60	0.19

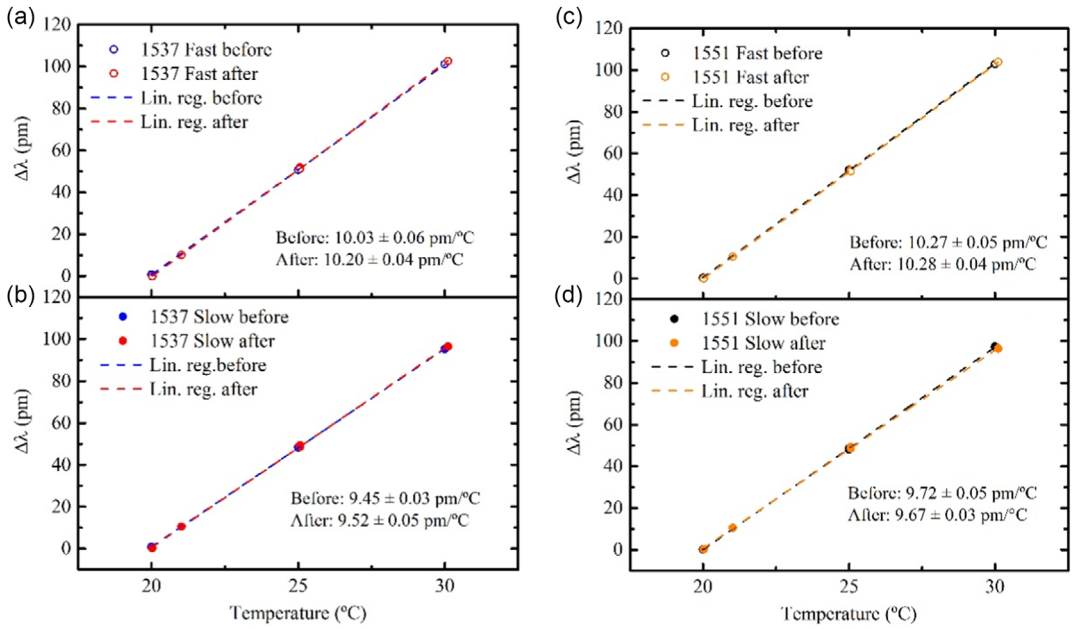

Figure 7. FBGs peak wavelength variation in function of temperature before and after the experiment. a,b) The FBG@1537 nm, fast and slow axis. c,d) The FBG@1551 nm fast and slow axis, respectively.

3.3. OFS Thermal Characterization Before and After 24 Months Period

After the experiment, for the FBG@1537 nm, the fast peak exhibited a temperature sensitivity of 10.03 ± 0.06 pm °C^{-1}, while the slow peak showed a sensitivity of 9.45 ± 0.03 pm °C^{-1}. Regarding the FBG@1551 nm, the fast peak sensitivity was 10.27 ± 0.05 pm °C^{-1}, and the slow peak sensitivity was 9.72 ± 0.05 pm °C^{-1}, the data used to calculate these sensitivities is presented in **Figure 7**. After the 24 month exposure to the electrolyte, the FBGs were recalibrated. The resulting values for the FBG@1537 nm were 10.20 ± 0.04 pm °C^{-1} for the fast peak and 9.52 ± 0.05 pm °C^{-1} for the slow peak, and for the FBG@1551 nm, the sensitivities were 10.28 ± 0.04 and 9.67 ± 0.03 pm °C^{-1}, respectively. The full data with the wavelength variation steps to temperature is reported in the (Figure S2, Supporting Information). These post-exposure calibrations demonstrate that the FBG sensors maintained their ability to respond to temperature changes, with no significant sensitivity variations and within the measurement error.

4. Conclusion

This study provides critical insights into the long-term stability of silica OFS in LiB electrolytes. Over a 24-month aging test, spectral monitoring, SEM, and EDS analyses confirmed that OFS maintained their structural integrity, with minor wavelength shifts attributed to external temperature fluctuations rather than material degradation. Birefringence analysis further corroborated the structural stability of the fibers throughout the experiment.

The thermal calibration of the FBG sensors before and after aging demonstrated consistent temperature response, with no significant deviations in sensitivity. SEM analysis revealed the formation of deposits on the fiber surfaces, including cubic-like $LiPF_6$ crystals appearing from month 3 and growing over time. Despite these deposits, no significant degradation of the silica fiber material or its diameter was observed, reinforcing the durability and robustness of OFS even under prolonged exposure to the harsh chemical environments of batteries. The mechanisms behind the formation of these deposits were not investigated in this study. Future studies could employ techniques such as inductively coupled plasma atomic emission spectroscopy or the Karl Fischer method to monitor electrolyte composition changes over time, particularly to assess silica leaching and moisture content, which can influence fiber degradation.

While these results highlight the robustness of OFS for battery monitoring applications, additional research is necessary to evaluate their performance in real LiB cells, where temperature variations, electrolyte decomposition, and mechanical stresses could impact sensor reliability. Future experiments should be conducted

under cycling and calendar aging conditions to comprehensively assess the long-term behavior of these sensors. However, the results demonstrate that the optical fiber sensor's performance remains unaffected by the electrolyte after more than 24 months at ambient temperature. Additionally, while the experimental setup provided valuable insights, conducting tests under more controlled conditions would further validate the findings.

In conclusion, silica-based OFS remain promising candidates for next-generation battery management systems due to their durability, accuracy, and resistance to harsh chemical environments. However, further validation in operational battery conditions is required to ensure their long-term reliability and industrial applicability.

Acknowledgements

The authors gratefully acknowledge the European Project "Innovative physical/virtual sensor platform for battery cell" (INSTABAT) (European Union's Horizon 2020 research and innovation program under grant agreement No 955930), https://www.instabat.eu/. INSTABAT is under the umbrella of BATTERY2030+ large-scale initiative under grant agreement N° 957213. This work was supported by project i3N (UIDB/50025/2020, UIDP/50025/2020, and LA/P/0037/2020), the LAQV-REQUIMTE (UIDB/50006/2020), and to the CICECO-Aveiro Institute of Materials (UID/CTM/50011/2019, UIDB/50011/2020, and UIDP/50011/2020), all financed by national funds through the Fundação para a Ciência e Tecnologia and the Ministério da Educação e Ciência of Portugal. The authors L.M., L.F.B.F., N.F.S., M.S.F., and M.S.N. are grateful for the grants 2023.01848.BD, SFRH/BD/150663/2020, 2022.04595. CEECIND, CEECINST/00013/2021/CP2779/CT0014, and 2022.07976. CEECIND/CP1720/CT0049, respectively.

Conflict of Interest

The authors declare no conflict of interest.

Keywords: analyses · electrolyte $LiPF_6$ · lithium–ion batteries · optical fiber sensor durabilities · scanning electron microscopy and energy-dispersive X-ray spectroscopy · sustainable energies

[1] B. Dunn, H. Kamath, J. M. Tarascon, *Science* **2011**, *334*, 928.
[2] L. Lu, X. Han, J. Li, J. Hua, M. Ouyang, *J. Power Sources* **2013**, *226*, 272.
[3] B. Diouf, R. Pode, *Renewable Energy* **2015**, *76*, 375.
[4] Y. Wang, J. Tian, Z. Sun, L. Wang, R. Xu, M. Li, Z. Chen, *Renewable Sustainable Energy Rev.* **2020**, *131*, 110015.
[5] X. Hu, F. Feng, K. Liu, L. Zhang, J. Xie, B. Liu, *Renewable Sustainable Energy Rev.* **2019**, *114*, 109334.
[6] Y. D. Su, Y. Preger, H. Burroughs, C. Sun, P. R. Ohodnicki, *Sensors* **2021**, *21*, 1397.
[7] G. Han, J. Yan, Z. Guo, D. Greenwood, J. Marco, Y. Yu, *Renewable Sustainable Energy Rev.* **2021**, *150*, 111514.
[8] J. Peng, X. Zhou, S. Jia, Y. Jin, S. Xu, J. Chen, *J. Power Sources* **2019**, *433*, 226692.
[9] J. Xi, J. Li, H. Sun, T. Ma, L. Deng, N. Liu, X. Huang, J. Zhang, *Sens. Actuators, A* **2022**, *347*, 113888.
[10] L. Matuck, J. L. Pinto, C. Marques, M. Nascimento, *Batteries* **2022**, *8*, 233.
[11] F. Freitas, L. Matuck, J. Bierlich, M. Ferreira, C. Marques, M. Nascimento, *J. Phys.: Conf. Ser.* **2022**, *2407*, 12023.
[12] L. C. Matuck, P. D. Cabrita, J. L. Pinto, C. A. Marques, *Batteries* **2023**, *2*, 2200046.
[13] L. Matuck, J. P. Santos, F. Freitas, L. B. Fontes, J. Bierlich, S. Geniès, J. Pinto, M. Ferreira, O. Raccurt, M. Nascimento, *Chem. Eng. J.* **2024**, *500*, 156806.
[14] J. Amici, P. Asinari, E. Ayerbe, P. Barboux, P. Bayle-Guillemaud, R. J. Behm, M. Berecibar, E. Berg, A. Bhowmik, S. Bodoardo, I. Castelli, I. Cekic-Laskovic, R. Christensen, S. Clark, R. Diehm, R. Dominko, M. Fichtner, A. Franco, A. Grimaud, N. Guillet, M. Hahlin, S. Hartmann, V. Heiries, K. Hermansson, A. Heuer, S. Jana, L. Jabbour, J. Kallo, A. Latz, H. Lorrmann, et al., *Adv. Energy Mater.* **2022**, *12*, 2102785.
[15] S. Ghashghaie, J. Bonefacino, Y. N. Cheung, X. Cheng, M. Wang, H. Y. Tam, J. Tarascon, S. Boles, *J. Electrochem. Soc.* **2024**, *171*, 040515.
[16] J. Huang, C. Delacourt, P. Desai, J. M. Tarascon, *J. Electrochem. Soc.* **2024**, *171*, 030516.
[17] Y. J. Ee, K. S. Tey, K. S. Lim, P. Shrivastava, S. B. R. S. Adnan, H. Ahmad, *J. Energy Storage* **2021**, *40*, 102704.
[18] S. Bandyopadhyay, M. Fabian, K. Li, T. Sun, K. T. V. Grattan, *Batteries* **2023**, *9*, 508.
[19] S. Liu, K. Li, *Trans. Inst. Meas. Control* **2023**, *45*, 1570.
[20] K. M. Alcock, M. Grammel, Á. González-Vila, L. Binetti, K. Goh, L. S. M. Alwis, *Sens. Actuators, A* **2021**, *332*, 113061.
[21] M. Nascimento, M. S. Ferreira, J. L. Pinto, *Measurement* **2017**, *111*, 260.
[22] W. Mei, Z. Liu, C. Wang, C. Wu, Y. Liu, P. Liu, X. Xia, X. Xue, X. Han, J. Sun, G. Xiao, H. Y. Tam, J. Albert, Q. Wang, T. Guo, *Nat. Commun.* **2023**, *14*, 1.
[23] B. Sun, Y. Wang, J. Qu, C. Liao, G. Yin, J. He, J. Zhou, J. Tang, S. Liu, Z. Li, Y. Liu, *Opt. Express* **2015**, *23*, 1906.
[24] J. Fleming, T. Amietszajew, E. Mcturk, D. P. Towers, D. Greenwood, R. Bhagat, *HardwareX* **2018**, *3*, 100.
[25] J. J. Unterkofler, R. R. Klambauer, A. Bergmann, in *Optica Sensing Congress 2023 (AIS, FTS, HISE, Sensors, ES)*, Optica Publishing Group, Munich, Germany **2023**, p. SW3D.3.
[26] S. Novais, M. Nascimento, L. Grande, M. Domingues, P. Antunes, N. Alberto, C. Leitão, R. Oliveira, S. Koch, G. Kim, S. Passerini, J. Pinto, *Sensors* **2016**, *16*, 1394.
[27] Instabat Project - Based on Battery 2030+ Group [Internet], https://www.instabat.eu/ (accessed: March 2024).
[28] Q. Q. Liu, X. X. Wang, J. J. Zhu, Y. Ou, in *2024 IEEE Transportation Electrification Conf. Expo, Asia-Pacific (ITEC Asia-Pacific)* Xian, China **2024**, p. 677.
[29] Y. Wu, X. Long, J. Lu, R. Zhou, L. Liu, Y. Wu, *J. Energy Storage* **2023**, *57*, 106207.
[30] A. Othonos, K. Kalli, G. E. Kohnke, *Phys. Today* **2000**, *53*, 61.
[31] G. Rego, *Sensors* **2023**, *23*, 6023.

Manuscript received: January 30, 2025
Revised manuscript received: March 17, 2025
Version of record online: March 21, 2025